Improving orientation, packing density and molecular arrangement in SAMs of bi-anchoring Ferrocene-triazole derivatives by 'Click' Chemistry

Vikas Jangid, Damien Brunel, Estéban Sanchez-Adaime, Anil Kumar Bharwal, Frédéric Dumur, David Duché, Mathieu Abel, Mathieu Koudia, Thierry Buffeteau, Christian A. Nijhuis, et al.

Improving orientation, packing density and molecular arrangement in SAMs of bi-anchoring Ferrocene-triazole derivatives by 'Click' Chemistry

Journal:	*Langmuir*
Manuscript ID	la-2022-002155.R1
Manuscript Type:	Article
Date Submitted by the Author:	17-Feb-2022
Complete List of Authors:	Jangid, Vikas; Aix-Marseille Universite, IM2NP; Aix-Marseille Universite, Madirel BRUNEL, Damien; Aix-Marseille-University, ICR Adaime, Esteban; Aix-Marseille Universite, IM2NP Bharwal, Anil Kumar; Aix-Marseille Université, IM2NP Dumur, Frederic; Aix-Marseille Université, ICR Duché, David; Aix-Marseille Universite, IM2NP Abel, Mathieu; Aix-Marseille Universite, IM2NP Koudia, Mathieu; Aix-Marseille Universite, IM2NP, Faculté des Sciences et Techniques Buffeteau, Thierry; Universite de Bordeaux, Institut des Sciences Moléculaires Nijhuis, Christian; National University of Singapore, Molecules and Materials Berginc, Gérard; Thales Research and Technology France, LEBOUIN, Chrystelle; Aix-Marseille University Faculty of Science, Escoubas, Ludovic; Aix-Marseille Universite, IM2NP

Improving orientation, packing density and molecular arrangement in SAMs of bi-anchoring Ferrocene-triazole derivatives by 'Click' Chemistry

Vikas Jangid [1,2], Damien Brunel [3], Esteban Sanchez-Adaime [1], Anil Kumar Bharwal[1], Frédéric Dumur [3], David Duché [1], Mathieu Abel[1], Mathieu Koudia[1], Thierry Buffeteau [4], Christian A. Nijhuis [5], Gerard Berginc[6], Chrystelle Lebouin [2] and Ludovic Escoubas[1*]

[1] Aix Marseille Univ, CNRS, Université de Toulon, IM2NP, UMR 7334, F-13397 Marseille, France
[2] Aix Marseille Univ, CNRS, MADIREL, UMR 7246, F-13397 Marseille, France
[3] Aix Marseille Univ, CNRS, ICR, UMR 7273, F-13397 Marseille, France
[4] Univ. Bordeaux, Institut des Sciences Moléculaires ISM, CNRS UMR5255, F-33405 Talence, France
[5] Hybrid Materials for Opto-Electronics Group, Department of Molecules and Materials, MESA+ Institute for Nanotechnology and Center for Brain-Inspired Nano Systems, Faculty of Science and Technology, University of Twente, 7500 AE Enschede, The Netherlands.
[6] Thales LAS OME, 78990, Elancourt, France.

***Corresponding author**
Ludovic Escoubas: ludovic.escoubas@univ-amu.fr
ORCID ID: 0000-0002-2033-1304

ABSTRACT

This work describes self-assembled monolayers (SAMs) of two ferrocene derivatives with two anchoring groups (at the bottom and at the top of the SAM) deposited on ultra-flat template stripped gold substrates by cyclic voltammetry and analyzed by complementary surface characterization techniques. The SAM of each molecule is deposited by three different protocols: direct deposition (1 step), Click reaction on surface (2 steps) and reverse Click reaction on surface (2 steps). The SAM structure is well-studied to determine the SAM orientation, SAM arrangement and ferrocene position within the SAM. Electron transfer kinetics have also been performed which agree with the quality of each SAM. With the help of two anchoring groups and Click-chemistry active functional groups, we have shown that the two molecules can be deposited by either end controlling the position of ferrocene. We further investigated the involvement of the triazole five membered ring in the electron transfer mechanism. We have found that a carbon spacer between ferrocene and triazole improves the SAM packing. This study enhances the understanding of tethering thiol and thiol

acetate anchoring groups on gold by controlled orientation which may help in development of functional molecular devices requiring two anchoring groups.

Keywords: Ferrocene SAM, Cyclic Voltammetry, CuAAC, Ellipsometry, XPS, PM-IRRAS

Introduction

Self-assembled monolayers (SAMs) of functional molecules tethered on an electrode surface [1] are extensively studied and exploited since several decades [2]. In particular, redox active SAMs have become the focus of intense research efforts due to the wide range of applications requiring these monolayers including interfacial electron transfer, [3–12] biosensing, [13–17] molecular electronics, [18–20], corrosion protection [21–23] and opto-photovoltaics. [24,25] Ferrocene (Fc) terminated alkanethiols tethered on gold surface are the most widely studied redox active SAMs since the pioneering works of Chidsey's [7,26] and ground-breaking works followed by others, [27,28]. Some of the factors making Fc very interesting for research are Fc's reversible one-electron oxidation-reduction transformation,[26] ease of synthesis, conjugation with diverse aromatic and aliphatic chains to form SAMs and modification of such high derivative SAMs and facile deposition on gold. These SAMs are made up of majorly four components: : a redox active Fc group, an aliphatic or aromatic spacer, a connector between Fc and the spacer, and an anchoring group that binds to the bottom electrode surface.[29] Performance of the SAM depends on each component such as the length of the spacer,[30,31] the choice of the anchoring group[32,33] and the connector[34]. Hence, each component that will be used to elaborate SAMs has to be carefully selected prior to self-assembly of the molecule on an electrode surface with regards to the desired application.

There are several methods to prepare single component or mixed SAMs. Often, direct soaking of the substrate in a functional molecular solution to obtain SAMs consisting of one component is performed. Two strategies are often used to prepare mixed SAMs: soaking of the substrate in a mixture of the SAM precursors of interest along with a diluent [4,7] or subsequent soaking of the substrate in a solution of the SAM precursor and diluent. [35] Mixed SAMs are often used, for example, to reduce interactions between the Fc moieties and to control the orientation of the Fc units to obtain ideal electrochemical behavior (ideal Nernstian behavior). The ideal Nernstian behavior for Fc alkanethiolates characterized with cyclic voltammetry shows five characteristics: (i) no peak shift during oxidation and deduction, *i.e.*, difference between oxidation peak potential (E_{PA}) and reduction peak potential (E_{PC}) is zero, $\Delta E_P = 0$, (ii) the anodic peak current (I_{PC}) is equal to cathodic peak current (I_{PA}), (iii) the peak current is proportional to the scan rate, ν, (iv) the full width at half maxima (FWHM) of the voltammetric peak, E_{FWHM}, is 90.6 at room temperature and (v) only one reversible redox wave is present. [3637] Kitagawa et al. [38] used single component monolayers of Fc based tripod-shaped trithiol molecules on polycrystalline Au(111) which showed an ideal redox behavior. In their work, each molecule was bound to Au by three thiol bonds and hence provided a

sufficient separation between neighboring molecules to avoid any inter-molecular interactions without the help of any non-functional diluent.

Another novel approach for depositing well packed monolayers with a controlled orientation consists in performing a Click reaction directly on the electrode surface via a copper catalyzed alkyne-azide cycloaddition (CuAAC) reaction.[39] The idea here is to first deposit alkyne/azide terminated alkyl/aryl chains along with a diluent to generate a well-organized SAM and then to click the Fc moiety functionalized with azide/alkyne on top of the aforementioned SAM via CuAAC reaction to form a triazole connector. The Click reaction carried out on surface ensures an efficient control of the molecular orientation and the diluent inhibits (or limits) the possible interactions between neighboring Fc moieties. Parallel to this, the use of a diluent in the SAM enables to efficiently separate the reactive alkyne/azide terminated alkyl/aryl chains and to take into account the bulkiness of the Fc moieties. As a result of this, efficiency of the Click reaction can be improved by reducing the steric hindrance of bulky Fc head groups.[40–42] Choice of the Click reaction to connect the Fc moieties to SAMs is motivated by the fact that this reaction can take place at room temperature, that the azide and alkyne functional groups are independently stable and do not react together without catalysts. Additionally, formation of the triazole group is irreversible and thermally stable, ensuring the chemical stability of the resulting Fc-modified SAMs.[40]

Despite these efforts, the ideal Nernstian behavior is rarely achieved and abnormalities such as peak broadening/narrowing,[7,43–45] peak splitting[44,46,47] and peak shifting [48] are frequently observed in cyclic voltammograms. Studies reveal that these abnormalities are majorly caused by interactions between different moieties (Fc-Fc, C-C, Fc-C, Fc-Au etc.), presence of Fc in different microenvironments and defects or disordered phases in SAMs [36,49,50]. In this study, we have extended the current knowledge on deposition and electrochemical behavior of SAMs based of Fc-alkanethiols fabricated in two steps and prepared with Fc derivatives bearing two anchoring groups. This study attends to the molecular electronics requirement of binding two electrodes to the same molecular entity with perfect control on the arrangement, the quality of the resulting SAMs and the position of the electroactive Fc moieties with respect to the metal surface.

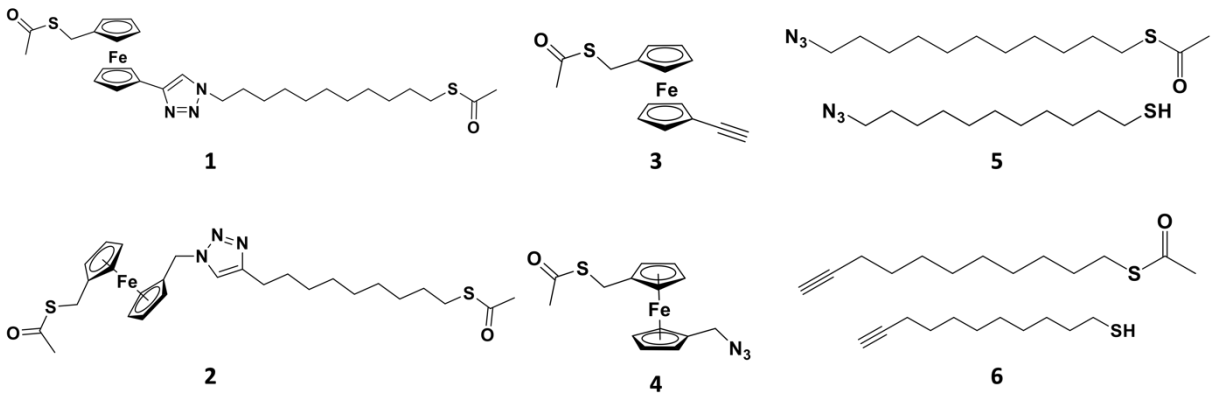

Figure 1. Chemical structures of the different alkyl chains and ferrocene derivatives used in this study.

Here, we studied two molecular rectifiers (molecules **1** and **2**) based on Fc derivatives (See Figure 1). The molecular rectifiers are composed of a redox active Fc moiety bearing two thiol

anchoring groups attached at both ends of the molecule. An alkyl chain is used as an insulating spacer and a triazole group acts as a connector between the alkyl chain and the Fc moiety. The difference between molecules **1** and **2** arises from the position of the triazole group with respect to the ferrocene moiety. Notably, in the case of molecule **2**, a -CH_2-group separates the Fc moiety from the triazole group whereas in the case of molecule **1**, the two parts are directly connected. Precursors of molecule **1**, *i.e*., Fc moiety (**3**) and dodecane thiol (**5**) are functionalized with alkyne and azide terminal groups, respectively. The position of these functionalities is reversed in the precursors used to prepare molecule **2**. Irrespective of the position of the azide and the alkyne groups, the two precursors used to prepare molecules **1** and **2** are joined or 'clicked' together via a CuAAC reaction forming irreversibly the triazole ring [51]. In the study, SAMs of these two molecules were deposited by following three distinct protocols: (1) in the first one, the molecules are 'clicked' in solution to form **1** and **2** and then directly deposited on ultra-flat template stripped gold Au^{TS} substrates. [52]; (2) The second protocol involves a Click reaction on surface [51]. First, thiols of **5** and **6** are self-assembled with octanethiol acting as a diluent to form well-organized SAMs on surface. Then, in a second step, the Click reaction allows to connect the second half of the molecular rectifier, namely molecules **3** and **4**; (3) Finally, in the third protocol, *i.e*., a 'reverse click reaction on surface' is applied, where the ferrocene derivatives 3 and 4 are first deposited on surface and by a Click reaction of alkyl chains **5** and **6**, the two molecular rectifiers can be totally formed. All the three deposition protocols used to deposit molecules **1** and **2** on substrates are summarized in Figure 2.

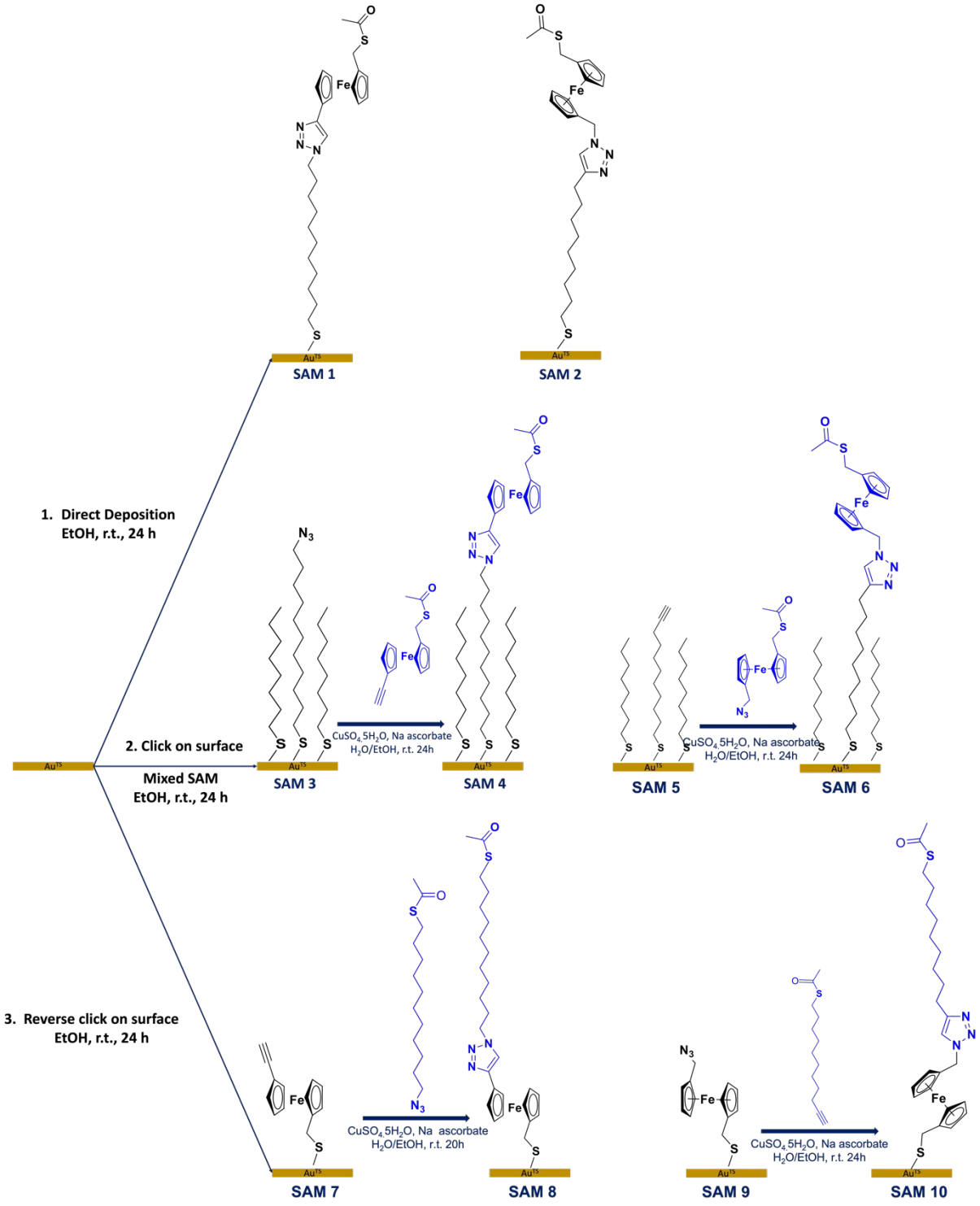

Figure 2. Scheme presenting the three strategies used to form SAMs with molecules 1 and 2 by (1) direct deposition (SAM 1 and SAM 2); (2) Click reaction on surface with diluent (SAM 3 to SAM 6) and (3) reverse Click reaction on surface (SAM 7 to SAM 10), respectively.

Apart from the cyclic voltammetric shape and electrochemical characteristics discussed above (E_{FWHM}, E_{pa}, E_{pc}, I_{pa} and I_{pa}), the surface molecular density Γ_{Fc} (mol/cm^2) of ferrocene derivatives and energy of highest occupied molecular orbital (E_{HOMO}) are also calculated with the help of equations 1 and 2, respectively.[47,53] In equation 1, Q_{tot} is half of the total charge

involved in one redox wave (calculated by integrating the oxidation and reduction waves and adding the area under these curves), *n* is number of electron transferred per molecule per redox cycle, *F* is Faraday constant and *A* is real surface area (here 0.5 cm^2) of the electrode (Au^{TS}) exposed to electrolyte solution. The theoretical value of Γ_{Fc} calculated for Fc alkanethiol considering Fc as a sphere of diameter 6.7 Å in hexagonal close packing is 4.5×10^{-10} mol/cm^2.[7] In equation 2, $E_{abs,NHE}$ is the absolute potential energy of the normal hydrogen electrode (-4.5 eV), and $E_{1/2,NHE}$ is the formal half-wave potential versus normal hydrogen electrode extracted from redox wave of CV (calculated by taking one half of the sum of E_{pa} and E_{pc}). To unravel the supramolecular SAM structure, we have employed the anodic peak deconvolution using Gaussian and Lorentzian functions reported by Lee et al.[54] and adopted by others.[36,49]

$$\Gamma_{Fc} = \frac{Q_{tot}}{nFA} \quad (1)$$

$$E_{HOMO} = E_{abs,NHE} - eE_{\frac{1}{2},NHE} \quad (2)$$

Here, we demonstrate the effect of the molecular structure and deposition protocol on the quality of the SAMs by analyzing the shape of the cyclic voltammograms and the different electrochemical parameters. We have carefully optimized the SAM deposition protocols and analyzed the resulting CV data to control and determine the molecular arrangements. We also address the effect of the triazole moiety on the performance of SAMs as it is the only difference from vastly studied Fc-alkanethiols. [2]–[29] Once formed, the different SAMs were investigated by complementary surface characterization techniques to precisely determine their thicknesses, the different elements present on surface and to identify the corresponding functional groups by ellipsometry, XPS (shown in supplementary information S1) and PM-IRRAS, respectively.

Experimental Section

Molecular synthesis:

All reagents and solvents were purchased from Aldrich, Alfa Aesar, Flurochem and TCI Europe and used as received without further purification. Mass spectroscopy was performed by the Spectropole of Aix-Marseille University. ESI mass spectral analyses were recorded with a 3200 QTRAP (Applied Biosystems SCIEX) mass spectrometer. The HRMS mass spectral analysis was performed with a QStar Elite (Applied Biosystems SCIEX) mass spectrometer. Elemental analyses were recorded with a Thermo Finnigan EA 1112 elemental analysis apparatus driven by the Eager 300 software. ^1H and ^{13}C NMR spectra were determined at room temperature in 5 mm o.d. tubes on a Bruker Avance 400 spectrometer of the Spectropole: ^1H (400 MHz) and ^{13}C (100 MHz). The ^1H chemical shifts were referenced to the solvent peak $CDCl_3$ (7.26 ppm) and the ^{13}C chemical shifts were referenced to the solvent peak $CDCl_3$ (77 ppm). Synthesis of molecules **1** and **2** and their precursors is reported in Brunel et al. [51] Each molecule was designed with two synthons synthetized independently, one containing a Fc group (**3** and **4**), and the other containing an alkane chain (**5** and **6**). The two synthons are joined together following CuAAC reaction between alkyne and azide functions forming triazole giving the whole molecules.

Substrates:

Ultra-flat template-stripped gold substrates were fabricated following the method reported in our previous study by Adaime et al. [52] Gold layer of thickness around 200 nm was deposited by e-beam evaporation on commercial Si(111) wafer followed by annealing at 400°C for 40 minutes . Glass pieces of dimension 1.5 × 1.5 cm were cleaned in distilled water, ethanol and finally isopropanol in an ultrasonic bath and dried under a nitrogen flow and put in an oxygen plasma for 30 seconds. Then, using a Norland61 ultraviolet (UV) curing optical adhesive, each piece of clean glass was glued to the wafer. The wafer was then placed under UV light for 1 hour to cure the adhesive. Each individual glass sample was then stripped from the wafer less than 30 s before being immersed in the molecular solution for SAM deposition.

SAM deposition:

For direct deposition (see Figure 2 (1)), a freshly template stripped Au^{TS} substrate was soaked in 1 mM degassed solution of molecule **1** or **2** for 20 hours in an inert environment. Click reaction on surface was implemented in two parts (see Figure 2 (2 & 3)). In the first step, SAMs of molecules **5** or **6** were deposited by soaking the substrate in 1 mM of mixed thiol degassed solution with octanethiol as a diluent in 1:1 ratio for 20 hours in inert environment. In the second step, molecules **3** or **4** were clicked on SAMs prepared in step 1 by soaking the substrate in 1 mM degassed solution (ethanol/water) of molecules **3** or **4** with 0.1 mM $CuSO_4.5H_2O$ and sodium ascorbate for another 20 hours in an inert environment. Inversed Click reaction on surface was followed in the similar way by first depositing molecules **3** or **4** (without diluent) and then clicking molecules **5** or **6** by CuAAC reaction.

Electrochemical analysis:

CV measurements were carried out in a custom-built electrochemical cell with three outlets at the top for degassing, counter electrode and reference electrode and one outlet at the bottom to assemble working electrode. A platinum wire was used as the counter electrode, an Ag/AgCl reference electrode and Au^{TS} served as the working electrode. Cyclic voltammograms were recorded in an aqueous solution of 1M $HClO_4$ using AUTOLAB PGSTAT302N potentiostat. NOVA 2 software was used to record CV between -0.1 to 0.9 V at a scan rate varying from 100 mV/s to1 V/s. The different SAMs were studied by CV where the redox curves *i.e*. cyclic voltammograms were analyzed. An ideal cyclic voltammogram was observed when the inter-molecular moieties do not interact with each other and the electron transfer rate was fast with respect to experimental time scale.[37] The ten SAMs shown in Figure 2 were studied by following the signature of an ideal cyclic voltammogram of one electron redox reaction. The characterization was followed by five characteristics of an ideal CV: (a) there was only one oxidation and one reduction wave *i.e*. one redox wave was present, (b) the full width of half maximum (E_{FWHM}) of redox wave was 90.6 mV at 25° C, (c) the difference between peak potentials of oxidation (E_{pa})and reduction (E_{pc}) is $\Delta E_p = 0$, (d) the peak anodic (I_{pa}) and cathodic (I_{pc}) peak currents were same and (e) proportional to scan rate ν. [62]

Kinetics study:

The kinetics of the electron transfer is calculated from the cyclic voltammograms measurements at different scan rates. By monitoring the oxidation and reduction potentials at each scan rate and by applying the Laviron method, the electron transfer rate constant (k_{et})

was measured [5]. The peak anodic (E_{pa}) and cathodic potentials (E_{pc}) were plotted vs. log ν to calculate the transfer coefficient a as shown in equation (3). The *x* intercepts of the lines from ν_a and ν_c were determined from this plot and inserted in the equation (4) to calculate k_{et}, where R, T, *n* and *F* has their usual values.

$$slope = -\frac{2.3RT}{\alpha nF} \quad (3)$$

$$k_{et} = \frac{\alpha nF\nu_c}{RT} = (1-\alpha)\frac{\alpha nF\nu_a}{RT} \quad (4)$$

Thickness measurement by Ellipsometry:
Variable Angle Ellipsometry (VASE) was used to determine the thicknesses of the SAMs deposited on Au substrate [63,64]. SAM modified Au substrates were exposed to an incident light for the wavelengths ranging between 400 and 650 nm at three different incident angles (65°, 70°, and 75°) and at five spots per sample. Semilab rotating compensator ellipsometer (RCE) with a micro-spot was used to focus the beam on the samples. Ellipsometric data were fit with the help of SEA software (Semilab) at the wavelength of 600 nm. The combined Drude−Lorentz oscillators dispersion law has been used to calculate the dielectric constant determination of gold substrate. The data analysis was performed based on a double determination of refractive indexes starting with a refractive index of 1.45 [65], and the SAM thickness which were precisely computed by iterative calculus until a $R^2 \approx 1$ value was reached. The acquired RMSE value from the fits for all incident angles were around 0.02 for all SAMs.

Polarization Modulation infrared reflection-absorption spectroscopy (PM-IRRAS):
PM-IRRAS spectra were recorded on a ThermoNicolet Nexus 670 FTIR spectrometer at a resolution of 4 cm^{-1}, by coadding several blocks of 1500 scans (30 minutes acquisition time). Experiments were performed at an incidence angle of 75° using an external homemade goniometer reflection attachment. The infrared parallel beam was directed out of the spectrometer with an optional flipper mirror and made slightly convergent with a first BaF_2 lens (191 mm focal length). The IR beams passed through a BaF_2 wire grid polarizer (Specac) to select the *p*-polarized radiation and a ZnSe photoelastic modulator (PEM, Hinds Instruments, type III). The PEM could modulate the polarization of the beam at a high fixed frequency, $2f_m$=100 KHz, between the parallel and perpendicular linear states. After reflection on the sample, the double modulated (in intensity and in polarization) infrared beam was focused with a second ZnSe lens (38.1 mm focal length) onto a photovoltaic MCT detector (Kolmar Technologies, Model KV104) cooled at 77 K. [66,67]

Results and discussion

Connector enables better SAM packing via direct deposition:
Before electrochemical analysis, XPS measurements were performed on the full SAMs of molecules **1** and **2** to identify the presence expected elements and to confirm the absence of any impurities. The results are shown in S1 in the supplementary information. Figure 6 shows the XPS analyses of carbon 1s, iron 2p, sulfur 2p, nitrogen 1s and oxygen 1s. Figure 3 shows the cyclic voltammograms of compounds **1** and **2** deposited by direct deposition and by Click

reactions on surface along with the proposed plausible molecular arrangements on Au^{TS}. The electrochemical characterizations of all SAMs are summarized in Table 1. SAM 2 shows an ideal behavior whereas peak broadening and splitting is observed in SAM 1 with a molecular density of Γ_{Fc} 4.63±0.6 × 10^{-10} mol/cm^2 and 2.58±0.9 × 10^{-10} mol/cm^2 and E_{FWHM} of 97±42 and 203±21 mV, respectively. To examine this difference in electrochemical behavior, we further investigated the curves presented in Figure 3A by deconstructing the anodic peak and fitting by a Gaussian and Lorentzian reported by Lee et al [54]. The deconvolution of the cyclic voltammogram of SAM 1 recorded at 1 V/s is shown in Figure 3B. We deconvoluted the two peaks, peak I, $E_{pa,I}$ (72% by area) and peak II, $E_{pa,II}$ (28% by area) with a fitting parameter R^2 of 0.98. These multiple peaks arise due to major differences in the microenvironment of the Fc moieties. In light of the claims published in the literature, the two peaks obtained by the deconvolution are assigned to ferrocene in standing up phase and buried phase, respectively. It is been reported that this defect is caused by the lattice mismatch between the atomic radii of sulfur and Fc moieties resulting into strain build-up forcing Fc moieties to accommodate in different microenvironments. [36] We relate $E_{pa,I}$ at lower oxidation potential of 442±19 mV to the Fc moieties which are standing up and in direct contact with the electrolyte solution (Figure 3B). We relate $E_{pa,II}$ detected at a higher oxidation potential of 593±23 mV to the buried Fc moieties partially shielded from the electrolyte solution. This relation is in agreement with the theory that exposed Fc moieties require less energy to oxidize than the shielded ones. Hence, the difference in oxidation potentials between $E_{pa,I}$ and $E_{pa,II}$ can be justified by these differences of environment for the ferrocene moieties.

Table 1. Electrochemical characterization of SAMs on gold substrate.

	E_{pa} (V)	E_{pc} (V)	ΔE (V)	Γ_{Fc} (× 10^{-10} mol/cm^2)	FWHM (V)	HOMO (eV)	K_{et} (s^{-1})
SAM 1	0.43	0.39	0.03	2.58±0.9	203±21	-5.14	126
SAM 2	0.45	0.39	0.06	4.63±0.6	97±42	-5.13	63
SAM 4	0.44	0.39	0.04	2.80±0.7	125±27	-5.06	94
SAM 6	0.41	0.36	0.03	1.92±0.4	165±18	-5.07	108
SAM 8	0.49	0.33	0.15	4.10±0.6	211±17	-5.14	25
SAM 10	0.49	0.40	0.08	3.71±0.8	186±21	-5.14	47

SAM 1 shows only 57% of surface area coverage whereas SAM 2 shows 100% area coverage as compared to the theoretical value of densely packed SAM. Despite similar molecular structures, the electrochemical behavior of **1** and **2** is very different from one another. Both molecules have odd number of carbon atoms in spacer part below triazole *i.e*. 11 and 9 respectively, which rules out possible odd-even effects.[36,49,57] We have shown graphically the plausible SAM structure of molecule **1** in Figure 3C where atomic strain between sulfur and Fc causes bending of the molecule and blocking the potential surface availability for other molecules [36]. This not only create two possible molecular arrangements but also reduces the molecular density to 57%. On the contrary, SAM 2 shows an ideal behavior with densely packed SAM of standing up molecules as shown in Figure 3F. In SAM 2, the strain build-up by the atomic size mismatch is accommodated by the carbon spacer between Fc and triazole enabling the Fc moieties to bend and coexists in the same molecular plane.

Alkyne in solution improves Click reaction yield on surface:

Figures 3G and 3J shows cyclic voltammograms of **1** and **2** deposited by Click reactions on the surface forming SAM 4 and SAM 6, respectively. Here, it is observed that the ideal behavior is reversed between **1** and **2** as compared to the previous section. The maximum area coverage for such type of deposition where the reaction is carried out on the surface is reported to be around 58% of the theoretically ideal value of a linear Fc alkanethiol monolayer with hexagonal packing.[7,41] SAM 4 shows a near ideal voltammogram with an area coverage Γ_{Fc} of $2.80\pm0.7 \times 10^{-10}$ mol/cm^2, *i.e.,* 62 % of the maximum coverage which is in agreement with the reported values. Due to the maximum Click yield on the surface and octanethiol as diluent, Fc units are separated and a plausible SAM structure is shown in Figure 3I. On the other hand, SAM 6 shows inferior area coverage Γ_{Fc} of $1.92\pm0.4 \times 10^{-10}$ mol/cm^2 which is only 42% of the theoretical maximum. It has been reported that that the yield of Click reaction on surface is better when an alkyne group is in solution and the azide group is immobilized on the surface.[41] The alkyne group is activated by the catalyst for the cycloaddition reaction with the azide group and the process is favorable when the alkyne group is in the solution phase. This interaction is easier when the alkyne is free in solution rather than tethered on the surface (where the movements are constraining).[68] SAM 4 shows a slight peak broadening with E_{FWHM} of 125±27 mV whereas SAM 6 shows a peak broadening and splitting with E_{FWHM} of 165±18 mV. We followed the peak deconvolution method similar to that mentioned in the last section for SAM 6 as shown in Figure 3K. The anodic peak is deconvoluted into peak I, $E_{pa,I}$ and peak II, $E_{pa,II}$. We relate $E_{pa,I}$ (83% by area) to standing up Fc moieties and $E_{pa,II}$ (17% by area) to disordered Fc moieties caused by unreacted alkyne groups and disordered phases as shown in Figure 3L. Due to the poor yield of the Click reaction, over one third of the alkyne groups remain unreacted causing a poor SAM packing.

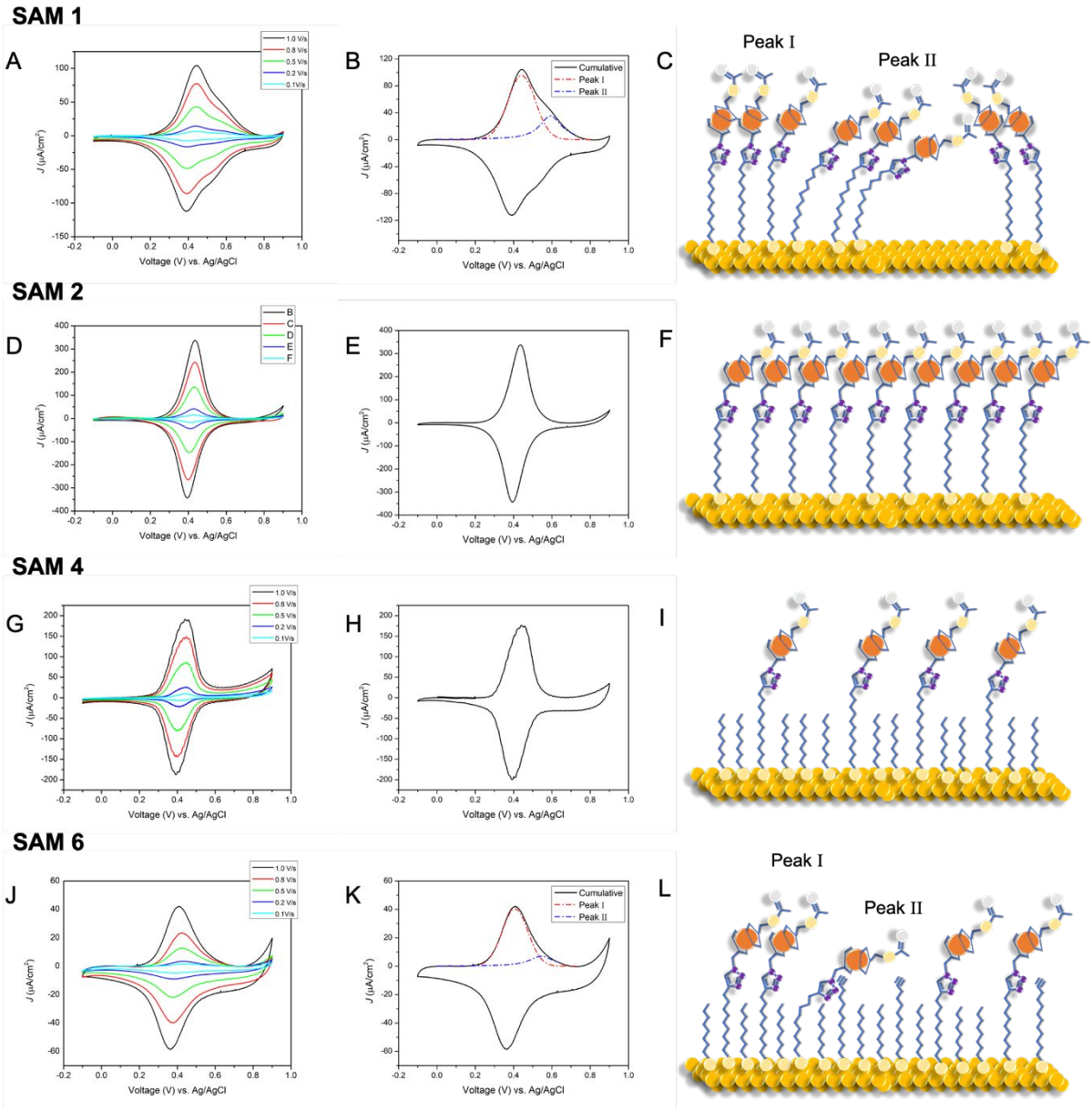

*Figure 3. CV of molecule **1** and **2** deposited on Au^{TS} by direct (SAM 1 and SAM 2) and click on surface (SAM 4 and SAM 6) protocols with current density on y-axis and potential on x-axis. A, D, G and J: Voltammogram taken at various scan rates vs. Ag/AgCl reference electrode for SAM 1, SAM 2, SAM 4 and SAM 6, respectively. B and K: Deconvolution of the voltammogram taken at the scan rate of 1 V/s for SAM 1 and SAM 6, respectively. E and H: Voltammogram taken at scan rate of 1 V/s showing an ideal curve for SAM 2 and SAM 3, respectively. Plausible graphical representation of SAM structure is shown in C, F, I and L.*

Reverse Click reactions on surface:

Molecules **1** and **2** have two anchoring groups at each terminal and until now the anchoring group located at the end of the carbon chain has been utilized for SAM deposition. In this section, we performed the deposition by rotating the molecules 180 degrees and joining by the thiol acetate located at the Fc end. Figure 4 shows the CV of the reverse Click reaction on the surface for SAM 8 and SAM 10. Here, the Fc moiety is first deposited followed by clicking of the carbon chain. To confirm the success of the Click reaction, a CV is recorded at each step. After the second step, the oxidation potential is anodically shifted by 100 mV as more energy is required to oxidize Fc moiety which is shielded from electrolyte solution by the carbon chain. Also, a decrease in the peak current density of around 70 µA is observed due to

desorption of few Fc moieties as longer chains are preferred than shorter chains. Surface area coverage Γ_{Fc} calculated for SAM 8 and SAM 10 is 4.10±0.6 × 10^{-10} mol/cm^2 and 3.71±0.8 × 10^{-10} mol/cm^2 respectively which is slightly lower than the theoretical value. Both the curves show peak broadening with peak potential E_{FWHM} values of 211±17 mV and 186±21 mV for SAM 8 and 10 respectively. This peak broadening can be explained by hybridization of the HOMO energy level at Fc with Au 4d orbitals because Fc is spatially located just one carbon away from the gold substrate.[36] The difference in peak potential ΔE_p for molecule **1** is increased from 50 to 110 mV and for molecule **2** from 30 to 90 mV when the orientation is reversed. This indicates that the rate of electron transfer decreases when Fc gets hybridized with Au and shielded from electrolyte solution by the carbon chain.

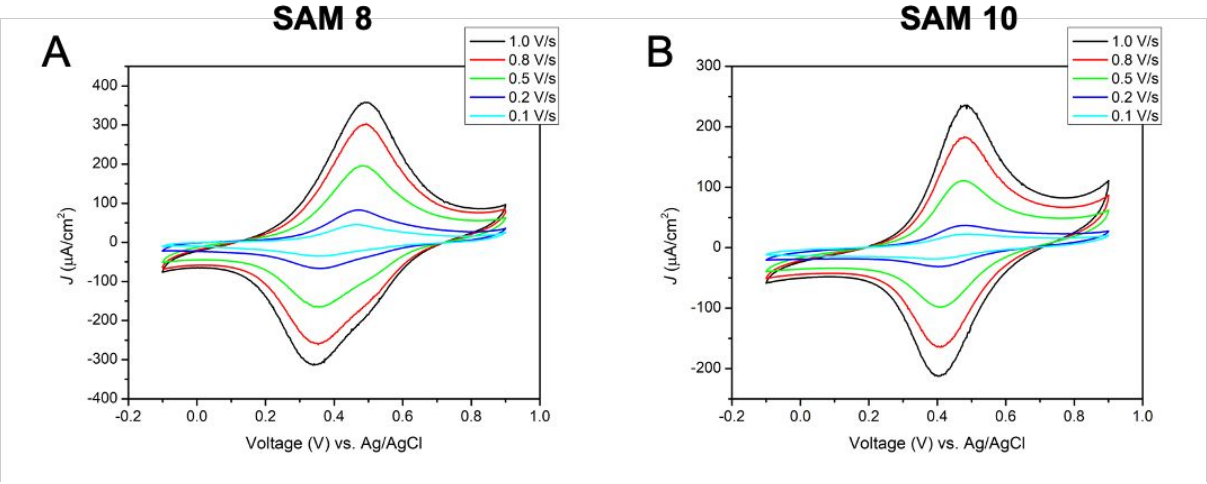

Figure 4. CV plots of SAM 8 and SAM 10 deposited by reverse click on surface of molecule 1 (A) and molecule 2 (B), respectively.

Effect of triazole moiety on HOMO position:

Fc alkanethiols are widely studied for various applications. Here, we take them as benchmark for the Fc derivatives discussed in this study.[2]–[29] The attractiveness of the molecules discussed here originates from their unique combination and facile implication *via* Click Chemistry. This not only allows us to control the position of the Fc moiety but also to study the SAM structure. However, to compare the molecules studied here with the Fc alkanethiols, we have to take into account the presence of the triazole moiety, which is a real novelty of our approach but can affect the electrochemical properties of our SAMs. Katritzky et al. reported that the HOMO and LUMO energy levels of the triazole are -10.35 and 0.48 eV, respectively.[69] Hence, the energy levels of triazole are far away from the HOMO of the Fc (~ -5 eV) and Fermi level of gold (~ -5.5 eV) and cannot participate in the electron-transfer mechanism. We further investigate the effect of the presence of the triazole on the HOMO of the Fc by electrochemical analysis as shown in Figure 5. The synthesis of molecules **B** and **C** are reported by Brunel et al. [51] We have started with the commercial Fc-11-dodecanethiol and compared E_{pa} and HOMO with Fc-derivatives including **1** and **2** as shown in Figure 5. Molecule **B** contains a triazole group placed four carbons away from Fc which shows no significant change in E_{pa} and HOMO values as compared to molecule A. We shifted the position of triazole next to Fc in molecule **C** and no significant changes are observed. Although a shift of 0.1 V and -0.1 eV is observed in E_{pa} and HOMO values respectively in **1** and **2**, these changes may have been caused by the presence of the thiol acetate group on top of the Fc causing an anodic

shift in the oxidation potential. Since no significant change was observed between **A** and **C**, this anodic shift is not induced by the presence of triazole.

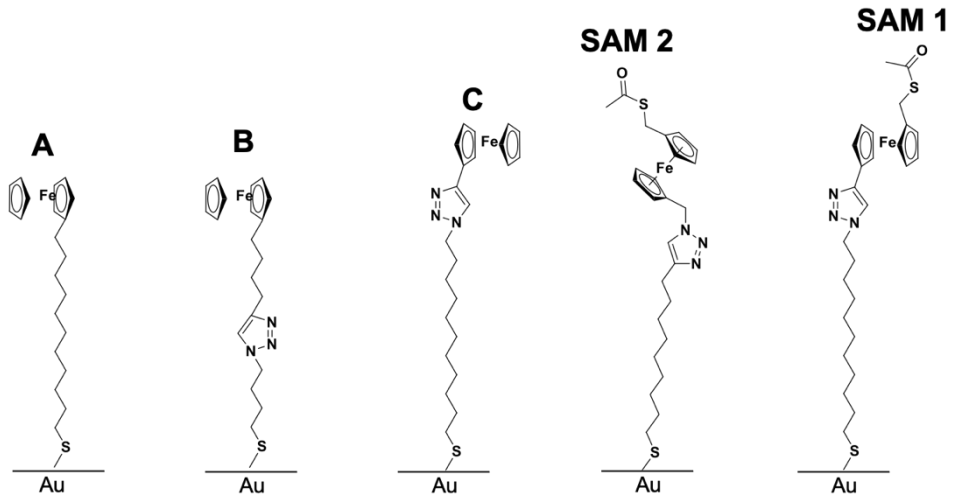

E_{pa} (V)	0.33	0.34	0.37	0.42	0.43
HOMO (eV)	-5.01	-5.02	-5.06	-5.13	-5.14

Figure 5. Anodic peak potential and corresponding HOMO of Fc-alkanethiol derivatives calculated by CV

Electron transfer kinetics:

Table 1 shows the electron transfer coefficient (K_{et}) of the full molecules in SAM 1, SAM 4 and SAM 8 for **1** and SAM 2, SAM 6 and SAM 10 for **2**. For molecule **1**, K_{et} ranges from 63 s^{-1} for direct deposition, 94 s^{-1} for the Click reaction on surface and 25 s^{-1} for the reverse Click reaction on surface. Similarly for **2,** K_{et} ranges from 126 s^{-1} for the direct deposition, 108 s^{-1} for the Click reaction on surface and 47 s^{-1} for the reverse Click reaction on surface. SAM 2 has a faster electron transfer than SAM 1 due to orderly arrangements of molecules, thanks to the carbon spacer. Both SAM 4 and SAM 6 has higher K_{et} due to control over orientation of ferrocene and reducing effects of neighboring Fc units through diluent and click on surface protocols. On the other hand, SAM 8 and SAM 10 have the lowest electron transfer rates due to the spatial position of ferrocene causing the hybridization of the HOMO involving in electron transfer with 4d orbital of gold. [36]

Ellipsometry thickness:

Table 2 summarizes the thickness measurement data on SAM 1 to SAM 10 with the corresponding refractive index to achieve a fitting parameter higher than 0.98. The height difference between SAM 1 and SAM 2 is 4 Å which strengthens our hypothesis on bending of the Fc units due to presence of a carbon spacer between the ferrocene and the triazole unit to release the strain build-up by the atomic size mismatch. The thickness of SAM 3 and SAM 5 coherently increases after Click reaction to form SAM 4 and SAM 6, respectively [70–72]. The difference of 3 Å between SAM 3 and SAM 5 is due to the fact that SAM 3 has 11 carbon atoms followed by three nitrogen atoms whereas SAM 5 has only 11 carbon atoms. Similarly, thickness of SAM 7 and SAM 9 increases consistently after reverse click reaction to form SAM 8 and SAM 9 respectively. The difference between the thickness of SAM 1, SAM 4 and SAM 8

with SAM 2, SAM 6 and SAM 10 for direct, Click reaction on surface and reverse Click reaction on surface, respectively, is consistent for all three deposition protocols.

Table 2. SAM thickness values and corresponding refractive indexes measured at 600 nm.

	Thickness (nm)	Refractive index at λ = 600 nm
SAM 1	2.2	1.46
SAM 2	1.8	1.46
SAM 3	1.1	1.49
SAM 4	2.1	1.48
SAM 5	0.8	1.53
SAM 6	2	1.45
SAM 7	1.1	1.51
SAM 8	2.1	1.51
SAM 9	0.9	1.98
SAM 10	1.8	1.46

PM-IRRAS analysis:

The different SAMs were further investigated by XPS to identify the expected elements and investigate the impurities (see supplementary information) followed by the PM-IRRAS to identify the functional groups present on the SAM modified Au substrates, modifications after Click reaction and to confirm the attachment of the Fc units to the carbon chain by Click on surface and reverse Click on surface reactions, respectively. Figure 6 shows the spectra of SAMs of molecule 1 in (A) and SAMs of molecule 2 in (B). Spectra of the direct deposited SAMs (SAM 1 and SAM 2) are plotted individually whereas spectra of the layers obtained by Click and reverse Click reactions on surface are overlapped for comparison. The bands detected at 2922, 2851 and 1465 cm^{-1} are assigned to asymmetric stretching modes ($\nu_a(CH_2)$), symmetric stretching modes ($\nu_s(CH_2)$) and the bending mode ($\delta(CH_2)$) of the methylene groups, respectively [72,73]. These three bands are marked on the spectra and are present in all the 10 SAMs. Bands at 3104 and 1106 cm^{-1} are assigned to the stretching mode νCH and the breathing ring mode νCC of the ferrocene group, respectively [74–76]. Finally, bands detected at 1689 cm^{-1} are assigned to stretching C=O mode of thio acetate group, at 2100 cm^{-1} to asymmetric stretching ν_aN_3 mode of azide group, at 3325 cm^{-1} and 2122 cm^{-1} to stretching ν(CH) and ν(C≡C) modes of alkyne group, respectively [72–76].

For SAM 1 and SAM 2, bands of methylene, ferrocene and carbonyl groups are detected whereas the bands that could correspond to the alkyne and azide groups are absent from the PM-IRRAS spectra, as expected. However, the frequency of the ν_aCH_2 mode for SAM 2 is 2925 cm^{-1}, which is 6 cm^{-1} higher than 2919 cm^{-1} corresponding to well-ordered SAMs. The frequency of ν_aCH_2 suggests the presence of some disorder of the alkyl chains in SAM 2 due to *gauche* defects [77]. In SAM 3, the band corresponding to the azide group at 2100 cm^{-1} is present and after Click reaction in SAM 4, the intensity of the azide band drastically decreased

and bands corresponding to ferrocene and the carbonyl group (attached to thiol acetate at the top) appears, which confirms the success of the Click reaction. Similarly, for SAM 5, bands corresponding to the alkyne group at 3325 cm^{-1} (νCH mode) and 2122 cm^{-1} (νC≡C mode) are present which completely disappears after Click reaction in SAM 6, with the appearance of new bands characteristics of ferrocene and the carbonyl group. SAM 8 contains bands of ferrocene and weak band of alkyne and after Click reaction, the alkyne band disappears and a new band corresponding to the carbonyl group appears, confirming the attachment of the carbon chain on top with the thiol acetate group. Similarly, in SAM 9, bands of azide and ferrocene are present and after Click reaction to form SAM 10, the intensity of the azide band decreases and a new band corresponding to the carbonyl group appears. However, the presence of azide bands in SAM 4, SAM 5 and SAM 10 reveals that the yield of Click reaction on surface is not 100 %, what was also reported by Collman and Béthencourt in previous works [40,41,65].

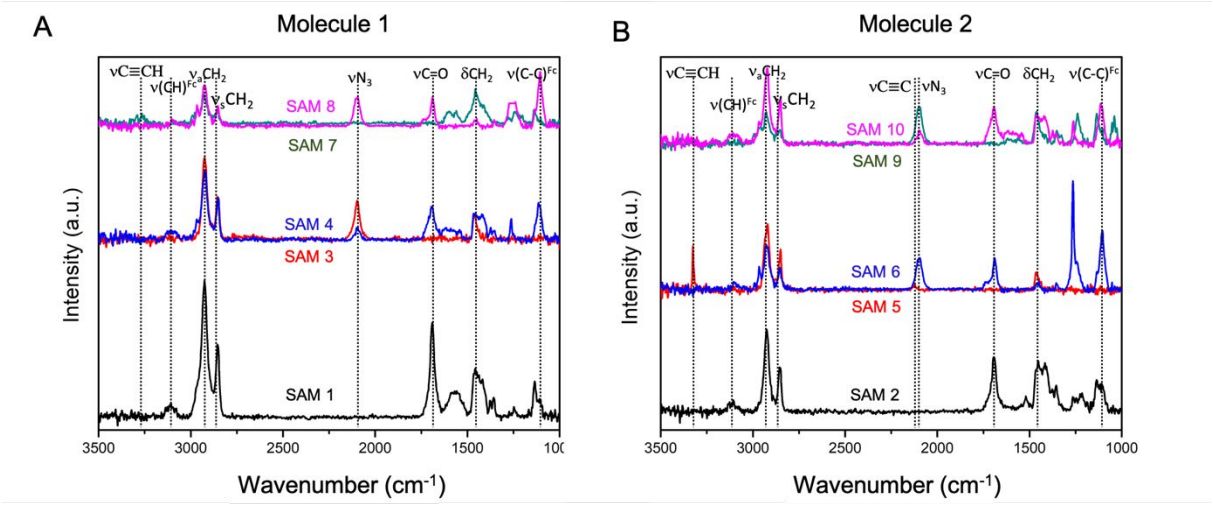

Figure 6. IRRAS spectra of SAMs of molecule 1 (A) and molecule 2 (B) with all the bands of functional groups marked by dotted lines.

Conclusions

Fc alkanethiols have been extensively studied since the early 90s for their unprecedented properties for various intrinsic and application-based studies. These studies and applications are majorly affected by the quality of SAMs in terms of packing and orientation of the individual molecules. Common challenge is to control the orientation of the molecule and the position of the Fc moiety within the SAM. Extensive researches have been done in the past decade to understand the electronic and supramolecular structures of SAMs and to explain the abnormalities [7,43–48]. To the best of our knowledge, not so much work has been done on Fc derivatives with two anchoring groups which are promising for applications in devices requiring sandwich-based architectures. Here, in the present study, we have addressed this by introducing two Fc derivatives and electrochemical investigated their SAM packing. The molecules are synthesized by CuAAC reaction which was performed both in solution and on

surfaces. SAMs of both the molecules formed by direct deposition and by Click reactions on surface were investigated and compared with each other. Molecule 1 shows a better SAM packing with a molecular orientation control when deposited via Click reaction on surfaces whereas the direct deposition yields SAMs that show peak splitting and broadening in the cyclic voltammograms. On the other hand, the opposite behavior is shown by molecule 2. We explain this difference in electrochemical behavior by the presence of the carbon spacer in molecule 2, which allows a better SAM packing whereas the Click reaction on surface yield is poor when the alkyne group is tethered first forming disordered phases. We have also shown control over the orientation of the molecule and the position of the Fc moiety within the SAM by reverse Click reaction on surface. Hence, by exploiting the versatility of CuAAC reaction and by integrating two anchoring groups at both ends of the molecule, we have improved both the orientation of the molecule and the position of Fc moiety. Kinetics of electron transfer rates follows a similar trend which emphasizes the necessity to control the order and orientation of the molecules.

CuAAC reaction takes place between alkyne and azide by forming a triazole moiety. We investigate the effect of the triazole ring on the HOMO energy level of the molecule which is centered at the Fc moiety. We compared the commercial Fc dodecanethiol with different Fc derivatives synthesized in our laboratory by CuAAC. Upon electrochemical determination of the anodic oxidation potential and HOMO, we observed a maximum difference of 100 mV in the oxidation potential due to differences in molecular structure and SAM packing. Hence, we conclude that the triazole ring does not alter the HOMO of Fc and that it is electrochemically inert in the potential range of the Fc activity.

The cyclic voltammetry results are in good agreement with the complementary surface characterization techniques performed in this work. Ellipsometry measurements revealed that the thickness of the respective SAMs are close to the expected values and confirm that the SAM thickness increases with the attachment of the second half of the molecule in the case of Click and reverse Click reactions on surface. XPS and PM-IRRAS further help to characterize the SAM obtained from the three deposition protocols in identifying the expected elements and functional groups and respective extend of Click Chemistry yield. This study can be beneficial for potential applications involving two anchoring units with an electron active group. Further works could focus on exploiting the different possible spatial arrangements of Fc units by modifying the precursors, electrical measurements to investigate the further potential of these kind of SAMs and simultaneously tethering two electrodes on each end of the molecules to mimic MIM (metal-insulator-metal) assemblies for several potential applications.

ASSOCIATED CONTENT

Supporting Information

For SAM samples, XPS analysis; C 1s XPS spectrum, Fe 2p XPS spectrum; S 2p XPS spectrum; N 1s XPS spectrum; O 1s XPS spectrum; no traces of impurities found in XPS spectrum

Notes

The authors declare no competing financial interest.

Acknowledgements

Vikas Jangid and Damien Brunel contributed equally to this work. This project has received funding from the European Union's Horizon 2020 research and innovation programme under the Marie Skłodowska-Curie grant agreement No713750. Also, it has been carried out with the financial support of the Regional Council of Provence- Alpes-Côte d'Azur and with the financial support of the A*MIDEX (n° ANR- 11-IDEX-0001-02), funded by the Investissements d'Avenir project funded by the French Government, managed by the French National Research Agency (ANR).). The Direction Générale de l'armement (DGA) is acknowledged for its financial support through the PhD grant of Damien Brunel.

References

(1) Wrighton, M. S. Surface Functionalization of Electrodes with Molecular Reagents. *Science (80-.).* **1986**, *231* (4733), 32–37.

(2) Love, J. C.; Estroff, L. A.; Kriebel, J. K.; Nuzzo, R. G.; Whitesides, G. M. Self-Assembled Monolayers of Thiolates on Metals as a Form of Nanotechnology. *Chemical Reviews*. American Chemical Society April 2005, pp 1103–1169.

(3) Fan, F. R. F.; Yang, J.; Cai, L.; Price, D. W.; Dirk, S. M.; Kosynkin, D. V.; Yao, Y.; Rawlett, A. M.; Tour, J. M.; Bard, A. J. Charge Transport through Self-Assembled Monolayers of Compounds of Interest in Molecular Electronics. *J. Am. Chem. Soc.* **2002**, *124* (19), 5550–5560.

(4) Weber, K.; Hockett, L.; Creager, S. Long-Range Electronic Coupling between Ferrocene and Gold in Alkanethiolate-Based Monolayers on Electrodes. *J. Phys. Chem. B* **1997**, *101* (41), 8286–8291.

(5) Laviron, E. General Expression of the Linear Potential Sweep Voltammogram in the Case of Diffusionless Electrochemical Systems. *J. Electroanal. Chem.* **1979**, *101* (1), 19–28.

(6) Smalley, J. F.; Feldberg, S. W.; Chidsey, C. E. D.; Linford, M. R.; Newton, M. D.; Liu, Y. P. Kinetics of Electron Transfer through Ferrocene-Terminated Alkanethiol Monolayers on Gold. *J. Phys. Chem.* **1995**, *99* (35), 13141–13149.

(7) Chidsey, C. E. D.; Bertozzi, C. R.; Putvinski, T. M.; Mujsce, A. M. Coadsorption of Ferrocene-Terminated and Unsubstituted Alkanethiols on Gold: Electroactive Self-Assembled Monolayers. *J. Am. Chem. Soc.* **1990**, *112* (11), 4301–4306.

(8) De Long, H. C.; Buttry, D. A. Ionic Interactions Play a Major Role in Determining the Electrochemical Behavior of Self-Assembling Viologen Monolayers. *Langmuir* **1990**, *6* (7), 1319–1322.

(9) Richardson, J. N.; Rowe, G. K.; Carter, M. T.; Tender, L. M.; Curtin, L. S.; Peck, S. R.; Murray, R. W. Electron Transfer Kinetics of Self-Assembled Ferrocene (C12)Alkanethiol Monolayers on Gold Electrodes from 125 K to 175 K. *Electrochim. Acta* **1995**, *40* (10), 1331–1338.

(10) Huck, H. Electrochemical Investigations of Mono- and Multilayers of Phenoxazine Dyes on Graphite Electrodes. *Phys. Chem. Chem. Phys.* **1999**, *1* (5), 855–859.

(11) Heimel, G.; Romaner, L.; Zojer, E.; Bredas, J. L. The Interface Energetics of Self-Assembled Monolayers on Metals. *Accounts of Chemical Research*. June 2008, pp 721–729.

(12) Wang, Q.; Evans, N.; Zakeeruddin, S. M.; Exnar, I.; Grätzel, M. Molecular Wiring of Insulators: Charging and Discharging Electrode Materials for High-Energy Lithium-Ion Batteries by Molecular Charge Transport Layers. *J. Am. Chem. Soc.* **2007**, *129* (11), 3163–3167.

(13) Campuzano, S.; Pedrero, M.; Pingarrón, J. M. A Peroxidase-Tetrathiafulvalene Biosensor Based on Self-Assembled Monolayer Modified {Au} Electrodes for the Flow-Injection Determination of Hydrogen Peroxide. *Talanta* **2005**, *66* (5), 1310–1319.

(14) Boozer, C.; Ladd, J.; Chen, S.; Jiang, S. DNA-Directed Protein Immobilization for Simultaneous Detection of Multiple Analytes by Surface Plasmon Resonance Biosensor. *Anal. Chem.* **2006**, *78* (5), 1515–1519.

(15) Chou, H. A.; Zavitz, D. H.; Ovadia, M. In Vivo CH3(CH2)11SAu SAM Electrodes in the Beating Heart: In Situ Analytical Studies Relevant to Pacemakers and Interstitial Biosensors. *Biosens. Bioelectron.* **2003**, *18* (1), 11–21.

(16) Chaki, N. K.; Vijayamohanan, K. Self-Assembled Monolayers as a Tunable Platform for Biosensor Applications. *Biosens. Bioelectron.* **2002**, *17* (1), 1–12.

(17) Kitagawa, K.; Morita, T.; Kimura, S. Electron Transfer in Metal-Molecule-Metal Junction Composed of Self-Assembled Monolayers of Helical Peptides Carrying Redox-Active Ferrocene Units. *Langmuir* **2005**, *21* (23), 10624–10631.

(18) Xiang, D.; Wang, X.; Jia, C.; Lee, T.; Guo, X. Molecular-Scale Electronics: From Concept to Function. *Chem. Rev.* **2016**, *116* (7), 4318–4440.

(19) Gehring, P.; Thijssen, J. M.; van der Zant, H. S. J. Single-Molecule Quantum-Transport Phenomena in Break Junctions. *Nat. Rev. Phys. 2019 16* **2019**, *1* (6), 381–396.

(20) Jeong, H.; Kim, D.; Xiang, D.; Lee, T. High-Yield Functional Molecular Electronic Devices. *ACS Nano* **2017**, *11* (7), 6511–6548.

(21) Zamborini, F. P.; Campbell, J. K.; Crooks, R. M. Spectroscopic, Voltammetric, and Electrochemical Scanning Tunneling Microscopic Study of Underpotentially Deposited Cu Corrosion and Passivation with Self-Assembled Organomercaptan Monolayers. *Langmuir* **1998**, *14* (3), 640–647.

(22) Jennings, G. K.; Laibinis, P. E. Self-Assembled n-Alkanethiolate Monolayers on Underpotentially Deposited Adlayers of Silver and Copper on Gold. *J. Am. Chem. Soc.* **1997**, *119* (22), 5208–5214.

(23) Ramachandran, S.; Tsai, B. L.; Blanco, M.; Chen, H.; Tang, Y.; Goddard, W. A. Self-Assembled Monolayer Mechanism for Corrosion Inhibition of Iron by Imidazolines. *Langmuir* **1996**, *12* (26), 6419–6428.

(24) Kim, J. S.; Park, J. H.; Lee, J. H.; Jo, J.; Kim, D.-Y.; Cho, K. Control of the Electrode Work Function and Active Layer Morphology via Surface Modification of Indium Tin Oxide for High Efficiency Organic Photovoltaics. *Appl. Phys. Lett.* **2007**, *91* (11), 112111.

(25) Knesting, K. M.; Hotchkiss, P. J.; MacLeod, B. A.; Marder, S. R.; Ginger, D. S. Spatially Modulating Interfacial Properties of Transparent Conductive Oxides: Patterning Work Function with Phosphonic Acid Self-Assembled Monolayers. *Adv. Mater.* **2012**, *24* (5), 642–646.

(26) Chidsey, C. E. D. Free Energy and Temperature Dependence. *Science (80-.).* **1991**, 919–922.

(27) Zheng, F.; Pérez-Dieste, V.; McChesney, J. L.; Luk, Y. Y.; Abbott, N. L.; Himpsel, F. J. Detection and Switching of the Oxidation State of Fe in a Self-Assembled Monolayer. *Surf. Sci.* **2005**, *587* (3), L191–L196.

(28) Viana, A. S.; Jones, A. H.; Abrantes, L. M.; Kalaji, M. Redox Induced Orientational

Changes in a Series of Short Chain Ferrocenyl Alkyl Thiols Self-Assembled on Gold(111) Electrodes. *J. Electroanal. Chem.* **2001**, *500* (1–2), 290–298.

(29) Kind, H.; Bonard, J. M.; Emmenegger, C.; Nilsson, L. O.; Hernadi, K.; Maillard-Schaller, E.; Schlapbach, L.; Forró, L.; Kern, K. Patterned Films of Nanotubes Using Microcontact Printing of Catalysts. *Adv. Mater.* **1999**, *11* (15), 1285–1289.

(30) Smith, C. E.; Odoh, S. O.; Ghosh, S.; Gagliardi, L.; Cramer, C. J.; Frisbie, C. D. Length-Dependent Nanotransport and Charge Hopping Bottlenecks in Long Thiophene-Containing π-Conjugated Molecular Wires. *J. Am. Chem. Soc.* **2015**, *137* (50), 15732–15741.

(31) Baghbanzadeh, M.; Bowers, C. M.; Rappoport, D.; Żaba, T.; Yuan, L.; Kang, K.; Liao, K. C.; Gonidec, M.; Rothemund, P.; Cyganik, P.; Aspuru-Guzik, A.; Whitesides, G. M. Charge Transport across Self-Assembled Monolayers of Oligo(Ethylene Glycol). *J. Am. Chem. Soc.* **2017**, *139* (22), 7624–7631.

(32) Jiang, L.; Yuan, L.; Cao, L.; Nijhuis, C. A. Controlling Leakage Currents: The Role of the Binding Group and Purity of the Precursors for Self-Assembled Monolayers in the Performance of Molecular Diodes. *J. Am. Chem. Soc.* **2014**, *136* (5), 1982–1991.

(33) Valkenier, H.; Huisman, E. H.; Van Hal, P. A.; De Leeuw, D. M.; Chiechi, R. C.; Hummelen, J. C. Formation of High-Quality Self-Assembled Monolayers of Conjugated Dithiols on Gold: Base Matters. *J. Am. Chem. Soc.* **2011**, *133* (13), 4930–4939.

(34) Song, P.; Yuan, L.; Roemer, M.; Jiang, L.; Nijhuis, C. A. Supramolecular vs Electronic Structure: The Effect of the Tilt Angle of the Active Group in the Performance of a Molecular Diode. *J. Am. Chem. Soc.* **2016**, *138* (18), 5769–5772.

(35) Eckermann, A. L.; Feld, D. J.; Shaw, J. A.; Meade, T. J. Electrochemistry of Redox-Active Self-Assembled Monolayers. *Coord. Chem. Rev.* **2010**, *254* (15–16), 1769–1802.

(36) Nerngchamnong, N.; Thompson, D.; Cao, L.; Yuan, L.; Jiang, L.; Roemer, M.; Nijhuis, C. A. Nonideal Electrochemical Behavior of Ferrocenyl-Alkanethiolate SAMs Maps the Microenvironment of the Redox Unit. *J. Phys. Chem. C* **2015**, *119* (38), 21978–21991.

(37) Bard, A. J.; Faulkner, L. R. *Electrochemical Methods: Fundamentals and Application*; Wiley: New York, US, 1989.

(38) Kitagawa, T.; Matsubara, H.; Komatsu, K.; Hirai, K.; Okazaki, T.; Hase, T. Ideal Redox Behavior of the High-Density Self-Assembled Monolayer of a Molecular Tripod on a Au(111) Surface with a Terminal Ferrocene Group. *Langmuir* **2013**, *29* (13), 4275–4282.

(39) Kolb, H. C.; Finn, M. G.; Sharpless, K. B. Click Chemistry: Diverse Chemical Function from a Few Good Reactions. *Angew. Chemie - Int. Ed.* **2001**, *40* (11), 2004–2021.

(40) Collman, J. P.; Devaraj, N. K.; Chidsey, C. E. D. "Clicking" Functionality onto Electrode Surfaces. *Langmuir* **2004**, *20* (4), 1051–1053.

(41) Collman, J. P.; Devaraj, N. K.; Eberspacher, T. P. A.; Chidsey, C. E. D. Mixed Azide-Terminated Monolayers: A Platform for Modifying Electrode Surfaces. *Langmuir* **2006**, *22* (6), 2457–2464.

(42) Ahmad, S. A. A.; Ciampi, S.; Parker, S. G.; Gonçales, V. R.; Gooding, J. J. Forming Ferrocenyl Self-Assembled Monolayers on Si(100) Electrodes with Different Alkyl Chain Lengths for Electron Transfer Studies. *ChemElectroChem* **2019**, *6* (1), 211–220.

(43) Creager, S. E.; Rowe, G. K. Redox Properties of Ferrocenylalkane Thiols Coadsorbed with Linear N-Alkanethiols on Polycrystalline Bulk Gold Electrodes. *Anal. Chim. Acta* **1991**, *246* (1), 233–239.

(44) Collard, D. M.; Fox, M. A. Use of Electroactive Thiols to Study the Formation and

Exchange of Alkanethiol Monolayers on Gold. *Langmuir* **1991**, *7* (6), 1192–1197.
(45) Uosaki, K.; Sato, Y.; Kita, H. Electrochemical Characteristics of a Gold Electrode Modified with a Self-Assembled Monolayer of Ferrocenylalkanethiols. *Langmuir* **1991**, *7* (7), 1510–1514.
(46) Rowe, G. K.; Creager, S. E. Chain Length and Solvent Effects on Competitive Self-Assembly of Ferrocenylhexanethiol and 1-Alkanethiols onto Gold. *Langmuir* **1994**, *10* (4), 1186–1192.
(47) Walczak, M. M.; Popenoe, D. D.; Deinhammer, R. S.; Lamp, B. D.; Chung, C.; Porter, M. D. Reductive Desorption of Alkanethiolate Monolayers at Gold: A Measure of Surface Coverage. *Langmuir* **1991**, *7* (11), 2687–2693.
(48) Creager, S. E.; Rowe, G. K. Competitive Self-Assembly and Electrochemistry of Some Ferrocenyl-n-Alkanethiol Derivatives on Gold. *J. Electroanal. Chem* **1994**, *370*, 203–211.
(49) Duffin, T. J.; Nerngchamnong, N.; Thompson, D.; Nijhuis, C. A. Direct Measurement of the Local Field within Alkyl-Ferrocenyl-Alkanethiolate Monolayers: Importance of the Supramolecular and Electronic Structure on the Voltammetric Response and Potential Profile. *Electrochim. Acta* **2019**, *311*, 92–102.
(50) Weidner, T.; Rössler, K.; Ecorchard, P.; Lang, H.; Grunze, M.; Zharnikov, M. Self-Assembled Monolayers of Ruthenocene-Substituted Biphenyl Ethynyl Thiols on Gold. *J. Electroanal. Chem.* **2008**, *621* (2), 159–170.
(51) Brunel, D.; Jangid, V.; Sanchez Adaime, E.; Duché, D.; Bharwal, A. K.; Abel, M.; Koudia, M.; Buffeteau, T.; Lebouin, C.; Simon, J. J.; Sauvage, R. M.; Berginc, G.; Escoubas, L.; Gigmes, D.; Dumur, F. Click Chemistry: An Efficient Tool to Control the Functionalization of Metallic Surfaces with Alkyl Chains Possessing Two Reactive End Groups. *Appl. Surf. Sci.* **2021**, *566*, 150731.
(52) Sanchez-Adaime, E.; Duché, D.; Escoubas, S.; Jangid, V.; Nony, L.; Moreau, A.; Lumeau, J.; Patrone, L.; Lebouin, C.; Escoubas, L. Atomic Force Microscopy and in Situ-Annealing X-Ray Diffraction Study on Template-Stripped Gold Substrates for Optimum Self-Assembled Monolayer Deposition. *Thin Solid Films* **2021**, 138978.
(53) Nijhuis, C. A.; Reus, W. F.; Whitesides, G. M. Mechanism of Rectification in Tunneling Junctions Based on Molecules with Asymmetric Potential Drops. *J. Am. Chem. Soc.* **2010**, *132* (51), 18386–18401.
(54) Lee, L. Y. S.; Sutherland, T. C.; Rucareanu, S.; Lennox, R. B. Ferrocenylalkylthiolates as a Probe of Heterogeneity in Binary Self-Assembled Monolayers on Gold. *Langmuir* **2006**, *22* (9), 4438–4444.
(55) Chen, J.; Reed, M. A.; Rawlett, A. M.; Tour, J. M. Large On-off Ratios and Negative Differential Resistance in a Molecular Electronic Device. *Science (80-.).* **1999**, *286* (5444), 1550–1552.
(56) Yuan, L.; Nerngchamnong, N.; Cao, L.; Hamoudi, H.; Del Barco, E.; Roemer, M.; Sriramula, R. K.; Thompson, D.; Nijhuis, C. A. Controlling the Direction of Rectification in a Molecular Diode. *Nat. Commun.* **2015**, *6*.
(57) Thuo, M. M.; Reus, W. F.; Nijhuis, C. A.; Barber, J. R.; Kim, C.; Schulz, M. D.; Whitesides, G. M. Odd-Even Effects in Charge Transport across Self-Assembled Monolayers. *J. Am. Chem. Soc.* **2011**, *133* (9), 2962–2975.
(58) Nerngchamnong, N.; Yuan, L.; Qi, D. C.; Li, J.; Thompson, D.; Nijhuis, C. A. The Role of van Der Waals Forces in the Performance of Molecular Diodes. *Nat. Nanotechnol.* **2013**, *8* (2), 113–118.

(59) Wang, L.; Yuan, L.; Jiang, L.; Yu, X.; Cao, L.; Nijhuis, C. A. Unraveling the Failure Modes of Molecular Diodes: The Importance of the Monolayer Formation Protocol and Anchoring Group to Minimize Leakage Currents. *J. Phys. Chem. C* **2019**, *123* (32), 19759–19767.

(60) Tour, J. M. Molecular Electronics Synthesis and Testing of Components. *Acc. Chem. Res.* **2000**, *33* (11), 791–804.

(61) Kitagawa, T.; Matsubara, H.; Okazaki, T.; Komatsu, K. Electrochemistry of the Self-Assembled Monolayers of Dyads Consisting of Tripod-Shaped Trithiol and Bithiophene on Gold. *Molecules* **2014**, *19* (9), 15298–15313.

(62) Kornilovitch, P. E.; Bratkovsky, A. M.; Stanley Williams, R. Current Rectification by Molecules with Asymmetric Tunneling Barriers. *Phys. Rev. B - Condens. Matter Mater. Phys.* **2002**, *66* (16), 1–11.

(63) Hitaishi, V. P.; Mazurenko, I.; Harb, M.; Clément, R.; Taris, M.; Castano, S.; Duché, D.; Lecomte, S.; Ilbert, M.; De Poulpiquet, A.; Lojou, E. Electrostatic-Driven Activity, Loading, Dynamics, and Stability of a Redox Enzyme on Functionalized-Gold Electrodes for Bioelectrocatalysis. *ACS Catal.* **2018**, *8* (12), 12004–12014.

(64) Hitaishi, V. P.; Clément, R.; Quattrocchi, L.; Parent, P.; Duché, D.; Zuily, L.; Ilbert, M.; Lojou, E.; Mazurenko, I. Interplay between Orientation at Electrodes and Copper Activation of Thermus Thermophilus Laccase for O2 Reduction. *J. Am. Chem. Soc.* **2019**, *142* (3), 1394–1405.

(65) Béthencourt, M. I.; Srisombat, L.; Chinwangso, P.; Lee, T. R. SAMs on Gold Derived from the Direct Adsorption of Alkanethioacetates Are Inferior to Those Derived from the Direct Adsorption of Alkanethiols. *Langmuir* **2009**, *25* (3), 1265–1271.

(66) Ramin, M. A.; Le Bourdon, G.; Daugey, N.; Bennetau, B.; Vellutini, L.; Buffeteau, T. PM-IRRAS Investigation of Self-Assembled Monolayers Grafted onto SiO 2/Au Substrates. *Langmuir* **2011**, *27* (10), 6076–6084.

(67) Desbat, B.; Blaudez, D.; Turlet, J. M.; Buffeteau, T. Calibration Procedure to Derive IRRAS Spectra from PM-IRRAS Spectra. *Appl. Spectrosc. Vol. 54, Issue 11, pp. 1646-1650* **2000**, *54* (11), 1646–1650.

(68) Worrell, B. T.; Malik, J. A.; Fokin, V. V. Direct Evidence of a Dinuclear Copper Intermediate in Cu(I)-Catalyzed Azide-Alkyne Cycloadditions. *Science (80-.).* **2013**, *340* (6131), 457–460.

(69) Katritzky, A. R.; Ramsden, C. A.; Joule, J. A.; Zhdankin, V. V. *Handbook of Heterocyclic Chemistry, Elsevier, Amsterdam,* **2010**,27-30.

(70) Biebuyck, H. A.; Bain, C. D.; Whitesides, G. M. Comparison of Organic Monolayers on Polycrystalline Gold Spontaneously Assembled from Solutions Containing Dialkyl Disulfides or Alkanethiols. *Langmuir* **2002**, *10* (6), 1825–1831.

(71) Bain, C. D.; Troughton, E. B.; Tao, Y. T.; Evall, J.; Whitesides, G. M.; Nuzzo, R. G. Formation of Monolayer Films by the Spontaneous Assembly of Organic Thiols from Solution onto Gold. *J. Am. Chem. Soc.* **2002**, *111* (1), 321–335.

(72) Porter, M. D.; Bright, T. B.; Allara, D. L.; Chidsey, C. E. D. Spontaneously Organized Molecular Assemblies. 4. Structural Characterization of n-Alkyl Thiol Monolayers on Gold by Optical Ellipsometry, Infrared Spectroscopy, and Electrochemistry. *J. Am. Chem. Soc.* **2002**, *109* (12), 3559–3568.

(73) Socrates, G. Biological Molecules - Macromolecules. *Infrared Raman Charact. Gr. Freq. Contents Tables Charts* **2001**, 328–340.

(74) Gryaznova, T. P.; Katsyuba, S. A.; Milyukov, V. A.; Sinyashin, O. G. DFT Study of

Substitution Effect on the Geometry, IR Spectra, Spin State and Energetic Stability of the Ferrocenes and Their Pentaphospholyl Analogues. *J. Organomet. Chem.* **2010**, *695* (24), 2586–2595.

(75) Duevel, R. V.; Corn, R. M. Amide and Ester Surface Attachment Reactions for Alkanethiol Monolayers at Gold Surfaces as Studied by Polarization Modulation Fourier Transform Infrared Spectroscopy. *Anal. Chem.* **2002**, *64* (4), 337–342.

(76) Diana, E.; Rossetti, R.; Stangheilini, P. L.; Kettle, S. F. A. Vibrational Study of (H5-Cyclopentadienyl)Metal Complexes. *Inorg. Chem.* **1997**, *36* (3), 382–391.

(77) Sang, L.; Mudalige, A.; Sigdel, A. K.; Giordano, A. J.; Marder, S. R.; Berry, J. J.; Pemberton, J. E. PM-IRRAS Determination of Molecular Orientation of Phosphonic Acid Self-Assembled Monolayers on Indium Zinc Oxide. *Langmuir* **2015**, *31* (20), 5603–5613.

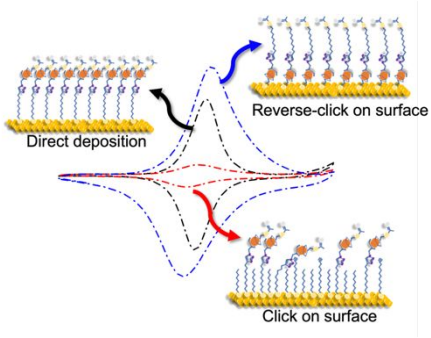

Figure. TOC graphic